Nanoscale Advances

ROYAL SOCIETY OF CHEMISTRY

PAPER

View Article Online
View Journal | View Issue

Cite this: *Nanoscale Adv.*, 2025, **7**, 5589

Annealing-induced optimization of green-synthesized ZnO nanoparticles for improved nanopriming in sustainable agriculture

Md. Shadman Mostafa, [abc] Samia Yeasmin, [d] Md. Mahmodul Hassan Pranto, [a] Syeda Maliha Reza, [a] Taslim Ur Rashid, [e] Harinarayan Das, [f] Mahmudur Rahman [g] and Ahsan Habib *[a]

Being a very simple and cost-effective way to improve crop growth, nanopriming has been widely adopted as an efficient and advanced technology in agriculture. In recent years, there has been a drive to use green synthesized metal oxide nanoparticles (NPs) for nanopriming, which promotes an eco-friendly approach to material synthesis. Among various factors that influence the properties of NPs, annealing plays a critical role in altering their structural and functional characteristics. However, the role of annealing in optimizing green-synthesized NPs for effective nanopriming remains largely unexplored. Here, we present the first report on the effect of annealing on green-synthesized ZnO NPs for effective nanopriming. We analyze surface morphology, crystallinity, elemental composition, and colloidal stability by varying the annealing temperature of as-synthesized ZnO NPs. We show that colloidally stable smaller NPs (annealed at 400 °C) exhibit optimal performance in nanopriming. This finding is supported by practical data showing a significant improvement in germination percentage (up to 61.7%) and shoot length (up to 85.3%) of *Momordica charantia* seeds treated with 120 mg L^{-1} of ZnO NP annealed at 400 °C. This study not only provides information on the specialized synthesis of ZnO NPs but also paves the way for sustainable agricultural practices to increase food production.

Received 14th April 2025
Accepted 26th July 2025

DOI: 10.1039/d5na00354g

rsc.li/nanoscale-advances

Introduction

The 2030 Agenda for Sustainable Development highlights the need for sustainable agriculture to address hunger and global food demands.[1,2] Feeding a projected 9.8 billion people by 2050 will require a 50% increase in food production from 2012 levels.[1,2] However, as global demographics are projected to increase, projections indicate that the growth of productive capacity per hectare will be slow.[3] In recent years, nanomaterials have emerged as promising tools, offering potential solutions to these challenges and enhancing crop yield.[4–6] In particular, seed nanopriming offers promising solutions to improve various aspects of plant growth, suppress diseases, and more.[7,8] Among various nanomaterials, ZnO has received considerable attention due to its beneficial effects on plant growth, disease resistance, crop yield, and secondary metabolism.[9–11] For efficient large-scale production of high-purity ZnO NPs, two synthesis approaches have been used: chemical and green synthesis.[12,13] Chemical synthesis methods come with significant drawbacks, including high costs and environmental impacts arising from the use of harsh chemicals.[14] Green methods are known for their biochemical diversity, nontoxic phytochemicals, and cost-effectiveness that offer advantages over chemical synthesis.[15] The biocompounds in leaf extracts, such as flavonoids and terpenoids, act as reducing and stabilizing agents in the synthesis of ZnO nanoparticles, offering additional advantages over chemical methods.[16–19]

The impact of nanomaterials on plant growth is influenced by their size, morphology, and surface properties. Yeasmin *et al.* demonstrated that smaller nanoparticles are more effective in enhancing plant growth and development.[20] Borgatta *et al.* found that nanoparticles with uniform structures exhibit greater efficiency compared to irregularly shaped nanoparticles.[21] Furthermore, they showed that negatively charged nanomaterials significantly reduced disease progression and increased biomass.[22] The size, morphology, and surface properties of green synthesized nanoparticles can be controlled

[a]*Department of Electrical and Electronic Engineering, University of Dhaka, Dhaka-1000, Bangladesh. E-mail: mahabib@du.ac.bd*
[b]*Department of Computer Science and Engineering, Daffodil International University, Dhaka-1216, Bangladesh*
[c]*Semiconductor Technology Research Centre, University of Dhaka, Dhaka-1000, Bangladesh*
[d]*Department of Robotics and Mechatronics Engineering, University of Dhaka, Dhaka-1000, Bangladesh*
[e]*Department of Applied Chemistry and Chemical Engineering, University of Dhaka, Dhaka-1000, Bangladesh*
[f]*Bangladesh Atomic Energy Commission, Dhaka-1000, Bangladesh*
[g]*Department of Electrical and Electronic Engineering, Dhaka University of Engineering & Technology, Gazipur-1707, Bangladesh*

through annealing, which decomposes biomolecular coatings.[23] Fig. 1 presents a schematic illustration of the green synthesis of ZnO nanoparticles, both with and without annealing. The green synthesis of ZnO involves naturally occurring reducing agents, such as flavonoids, which interact with metal ions, such as Zn^{2+} through their hydroxyl or carbonyl groups to form stable metal–ligand complexes. These complexes undergo chemical reactions with dissolved oxygen, leading to the formation of ZnO nanoparticles (see Fig. 1(I)).[24–27] Flavonoids serve both as reducing agents that facilitate nanoparticle formation and as stabilizers that prevent aggregation by coating the nanoparticle surfaces. Without heat treatment, this coating can result in irregular shapes and sizes.[28] Conventionally, annealing at high temperatures enhances crystallinity, which, in turn, increases the size of nanoparticles.[29,30] However, low-temperature annealing can yield nanomaterials with reduced size due to the decomposition of biocompounds, a more uniform morphology, and more negative surface potentials (see Fig. 1(II)).[23,28,31] Despite the well-established significance of size, morphology, and surface charge optimization for nanopriming, to the best of our knowledge, the role of annealing in reducing the size of green-synthesized nanoparticles for enhanced nanopriming efficiency remains unexplored.

Here, the use of annealing to optimize green-synthesized ZnO nanoparticles for enhanced nanopriming in agriculture was explored. To demonstrate the effect of annealing, ZnO nanoparticles were synthesized using *Azadirachta indica* (neem) leaf extract. The leaf extract contains reducing agents, including phytochemicals and enzymes, which facilitate green synthesis of ZnO nanoparticles.[32] It also acts as a stabilizer, preventing the agglomeration of nanoparticles.[33] Through characterization techniques to analyze the size, morphology, and surface charge, we show that annealing of the nanoparticles at temperatures between 200 °C and 400 °C reduces the size, particularly at 400 °C, resulting in the smallest size, the most uniform shape, and the most negative zeta potential of the ZnO nanoparticles. The effects of these nanoparticles on seed germination and seedling growth in *Momordica charantia* were assessed. Our study demonstrates the significant potential of annealed ZnO nanoparticles, especially at a concentration of 120 mg L^{-1} annealed at 400 °C, in enhancing seed germination by up to 61.7% and seedling growth by increasing shoot length by up to 85.3% compared to as-synthesized ZnO NPs. These findings offer valuable insight into the promising role of ZnO nanoparticles in sustainable agriculture.

Materials and methods

Materials

The materials used in this study included zinc acetate dihydrate ($Zn(CH_3COO)_2 \cdot 2H_2O$) as precursors and sodium hydroxide (NaOH) as coprecipitant. Zinc acetate dihydrate and sodium hydroxide were purchased from Sisco Research Laboratories and Loba Chemie, India, respectively. Deionized (DI) water and ethanol (C_2H_5OH) were used as solvents. All chemicals and reagents were of analytical grade and were utilized as received without additional purification. The leaves of the neem plant were collected from the Dhaka University Campus, Dhaka, Bangladesh.

Methods

Preparation of neem leaf extract. 15 g of neem leaves were washed thoroughly with plenty of DI water, and both surfaces of the leaves were sterilized with alcohol by gently rubbing. These leaves were heated for 2 hours in 100 mL of DI water at 60 °C.[34] The extract was then filtered with Whatman filter paper (pore size: 11 μm). The filtrated extract was stored in a cool and dry place for further use.

Green synthesis of ZnO NPs. The protocol developed by Singh *et al.* was adopted for the synthesis of ZnO nanoparticles, with further modifications.[35] In brief, 10 mL of plant extract was heated to 35 °C for 10 minutes, followed by the addition of

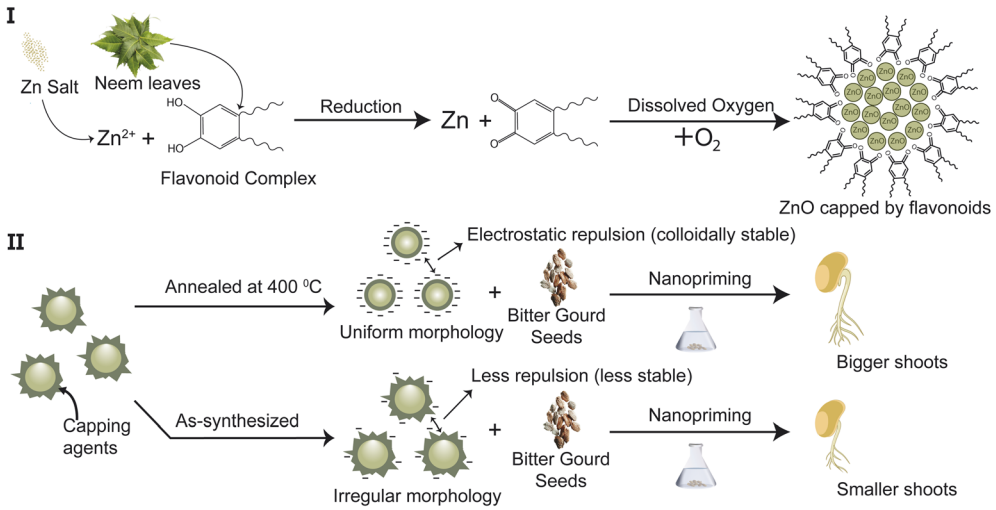

Fig. 1 Schematic illustration of (I) the green synthesis of ZnO nanoparticles and (II) the nanopriming process.

50 mL of 1 M zinc acetate solution and 25 mL of 2 M sodium hydroxide under stirring. An additional 10 mL of sodium hydroxide was added after 30 minutes, and the mixture was continuously stirred for approximately 2 hours at 35 °C until a white precipitate formed. The resulting solution was filtered using Whatman filter paper. Subsequently, the filtrate was washed four times with DI water and four times with ethanol. Each wash cycle involved centrifugation at 5000 rpm for 8 minutes. After drying in an oven at 60 °C for 12 hours, the product was pulverized for 1.5 hours using a mortar and pestle. The final powder was divided into four portions and annealed at 200 °C, 300 °C, 400 °C and 500 °C for 2 hours each, then stored in airtight containers for further experimentation. The samples were labeled as T-as (as synthesized), T-200 (annealed at 200 °C), T-300 (annealed at 300 °C), T-400 (annealed at 400 °C), and T-500 (annealed at 500 °C), respectively.

Characterization of ZnO NPs. The synthesized samples were characterized using various analytical techniques. X-ray diffraction (XRD) patterns were obtained using a high-temperature X-ray diffractometer (model: PW 3040-X'Pert PRO Philips). XRD analysis used Cu K_α radiation ($\lambda = 0.15418$ nm) in a range spanning from 10° to 80°. Morphological analysis was conducted using field emission scanning electron microscopy (FESEM), using the "high-resolution FESEM from the ZEISS Sigma family". An energy dispersive X-ray analysis was performed using the same equipment. Fourier transform infrared (FTIR) spectra were obtained using an "IR prestige-21, SHIMADZU", which covers the wavenumber range of 4000 to 400 cm^{-1}. The surface chemistry of the samples was analyzed by X-ray photoelectron spectroscopy (XPS) using a Thermo Fisher Scientific XPS spectrometer (7×10^{-7} mbar pressure) with monochromatic Al K_α radiation (1486.68 eV). The samples in powdered form were mixed with ethanol and then drop-cast onto a 1 × 1 cm slide glass, which was subsequently inserted into the spectrometer for analysis. Furthermore, UV-vis absorbance measurements were conducted using a "UV-2600i UV-Vis-NIR spectrometer, SHIMADZU", which covered wavelengths ranging from 200 to 800 nm. Dynamic light scattering (DLS) measurements were employed to determine the hydrodynamic size and zeta potential of the samples using a "Nanopartica SZ-100, HORIBA".

Seed treatment with ZnO NP priming solution. ZnO nanoparticle solutions were prepared at various concentrations (60, 120, 250, and 500 mg L^{-1}) by dispersing the nanoparticles in DI water and subjecting the solution to 30 minutes of ultrasonication. Healthy seeds of bitter gourd (*Momordica charantia*) were chosen for the priming treatment. Bitter gourd was selected due to its characteristic thick seed coat.[36] Seeds with an 80% germination rate were obtained as certified seeds from the Bangladesh Agricultural Development Corporation (BADC). In the seed priming process, seeds were submerged in the priming solutions for 48 hours. In contrast, seeds immersed in DI water were designated as the hydropriming group (control).

The bitter gourd seed germination assay with ZnO nano-primed and hydroprimed (control) was carried out using the paper towel technique, according to ISTA guidelines.[37] A sterile tissue paper was placed inside a plastic Petri dish (90 × 15 mm), and 150 seeds of each test and control were kept in the Petri dishes. The tissue paper was then moistened with DI water. The seeds were placed in the dark for germination at a temperature of 28 ± 2 °C. Germination was assessed by monitoring the emergence of the radicle. Observations were made every 24 hours for a span of ten days. To prevent the seeds from drying out, 5 mL of DI water was added to each Petri dish every other day. The number of germinated seeds was recorded daily, and the length of the seedling shoots was measured under a microscope. The experiment was carried out with three replicates, and the values were expressed as a mean.

Statistical analysis. A one-way ANOVA was performed on the treatment samples with three replicates, utilizing IBM SPSS Statistics version 27 for data analysis. The results are presented as mean ± standard error of the mean (SEM). The significance levels for all measured traits were determined, and means were compared using a two-tailed independent samples Student's *t*-test. Origin 2021 software was used for data visualization and graph generation.

Results and discussion

Green synthesis of ZnO nanoparticles

For enhanced performance of nanoparticles (NPs) as seed priming agents, it is crucial to utilize smaller, uniformly shaped NPs with superior surface stability.[38] Annealing could effectively reduce the size of the particles, enhance the morphological uniformity, and improve the stability of the colloids. To investigate the influence of annealing on size reduction, uniform morphology, and improved colloidal stability, ZnO NPs were synthesized using a green synthesis route. A qualitative analysis of ZnO NPs was performed by visually observing colorimetric changes.[39] The neem leaf extract changed from green to white after 2 hours of exposure to the Zn salt precursor at room temperature, indicating the bioreduction of zinc ions to ZnO NPs.[40] The color change happened due to the bulk exciton absorption in ZnO NP.[32,39,41] To confirm this, UV-vis absorption spectroscopy is used (Text S1). Fig. S1a shows the room temperature optical absorption spectra of as-synthesized ZnO NPs that exhibit a prominent and distinct absorption peak centered around 374 nm. This observation is consistent with previous research findings.[32] Moreover, the absence of additional peaks in the absorption spectra further supports the successful synthesis of pure ZnO powder.[42] Continuing our analysis, energy-dispersive X-ray spectroscopy (EDX) was employed to confirm the elemental composition of the constituent atoms and detect if there are any foreign impurity atoms. The strong signals corresponding to zinc and oxygen in the EDX spectrum (Fig. S1b) confirm the successful green synthesis of pure ZnO nanostructures using neem leaf extract.[32,39] The presence of a carbon (C) peak in the spectrum is attributed to capping agents such as flavonoids.[43] A blank experiment was performed following the described synthesis procedure, excluding the addition of neem extract. As shown in Fig. S1c, no characteristic ZnO absorption peak is observed, confirming that ZnO formation does not occur in the absence of a reducing agent.

Annealing-driven optimization of ZnO NPs for nanopriming

Elemental characterization

X-ray photoelectron spectroscopy. To investigate the surface electronic structure, composition, and bonding configuration of the T-400 ZnO NP sample, X-ray photoelectron spectroscopy (XPS) was conducted. The survey spectrum in Fig. 2a confirmed the presence of Zn, O, and C in the T-400 sample. The deconvoluted spectrum in Fig. 2b shows two peaks at 1021 eV and 1044 eV, which were assigned to Zn $2p_{3/2}$ and Zn $2p_{1/2}$, respectively.[44] This confirms the presence of Zn^{2+} in the oxidation state and indicates that the capping agents did not alter the chemical state of ZnO NPs.[45] The three deconvoluted peaks for O 1s in Fig. 2c correspond to the O^{2-} state of ZnO lattice oxygen (at 530 eV), the O^{2-} state of oxygen defects or vacancies (at 532 eV), and organic oxygen, which was assigned to the capping agents (at 533 eV).[46,47] The signals in the C 1s region of the reference ZnO shown in Fig. 2d were deconvoluted into C–C, C–O–C, and O–C=O peaks.[46] These peaks confirm the presence of organic materials, *e.g.*, capping agents, on the NP surface.

Fourier transform infrared spectroscopy. To evaluate the chemical composition and purity of the as-synthesized and annealed ZnO NPs, FTIR spectroscopy was conducted at room temperature. A reference spectrum of *Azadirachta indica* leaf extract is used to confirm the presence of bioactive compounds in the extract (see Fig. 3a). Fig. 3b displays the FTIR spectra of the as-synthesized and annealed ZnO NPs. Different bands in the spectra indicate the characteristic functional groups present in the material. A relatively wide band observed at 3422 cm^{-1} represents the fundamental stretching vibration of the O–H bond of the hydroxide group or the moisture adsorbed on the surfaces, which decreases consistently after annealing at higher temperatures.[48] This band can be attributed to several factors. Firstly, H^+ ions in the environment readily interact with O^{2-} anions within the ZnO hexagonal lattice, leading to the formation of O–H bonds. Secondly, residual hydroxyl (OH) groups present in the raw materials can also contribute to this band through electrostatic interactions with Zn^{2+} cations.[49] The peaks in the 415 to 520 cm^{-1} range correspond to the Zn–O stretching vibration modes, confirming the complete transformation of zinc acetate into zinc oxide.[49] In contrast, the medium-intense bands at 1390 cm^{-1} and 1560 cm^{-1} may correspond to the stretching vibrations of the bonds (–C=O) and (–C=C), respectively.[48,50] These vibrational bands, associated with functional groups such as (–C=O) and (–C=C), likely originate from compounds like flavonoids and terpenoids. These compounds can act as efficient capping and stabilizing agents for the obtained ZnO NPs.[32,39] Here, the decreasing trend of the peak intensity at 1390 cm^{-1} and

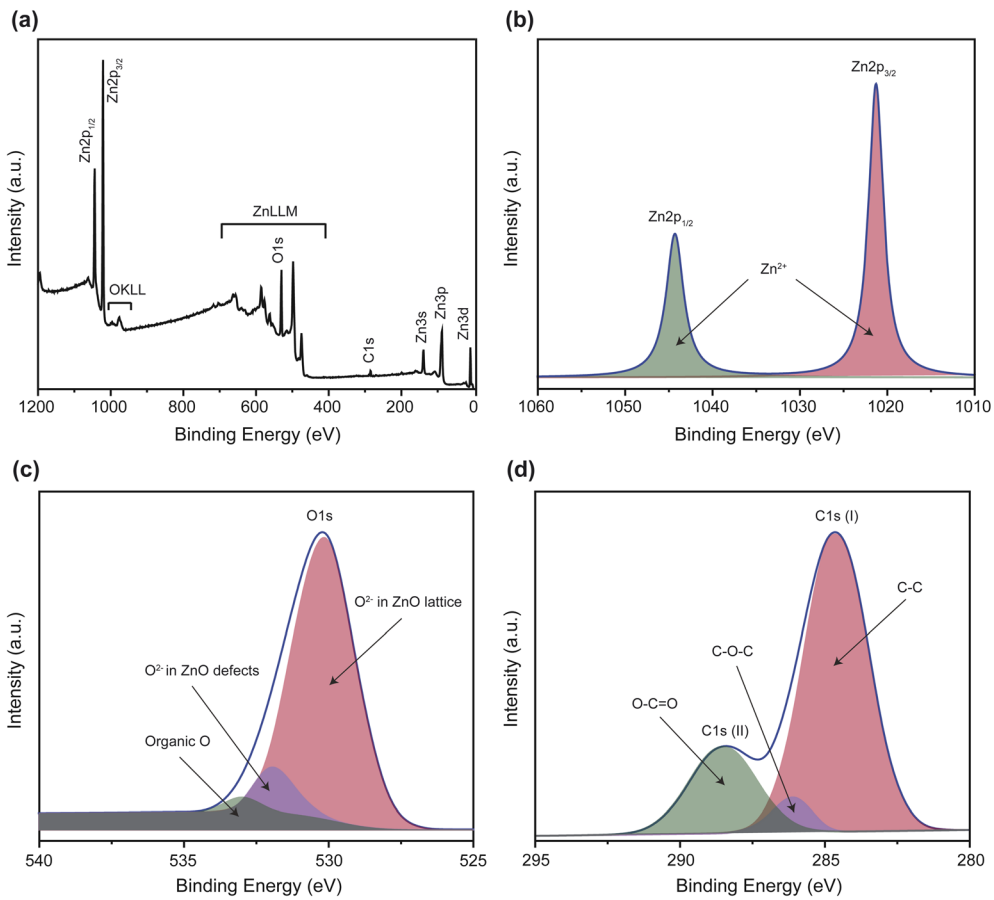

Fig. 2 XPS spectra of green synthesized ZnO NPs annealed at 400 °C: (a) survey spectrum and high-resolution deconvoluted XPS spectra for (b) Zn, (c) O, and (d) C in the T-400 sample.

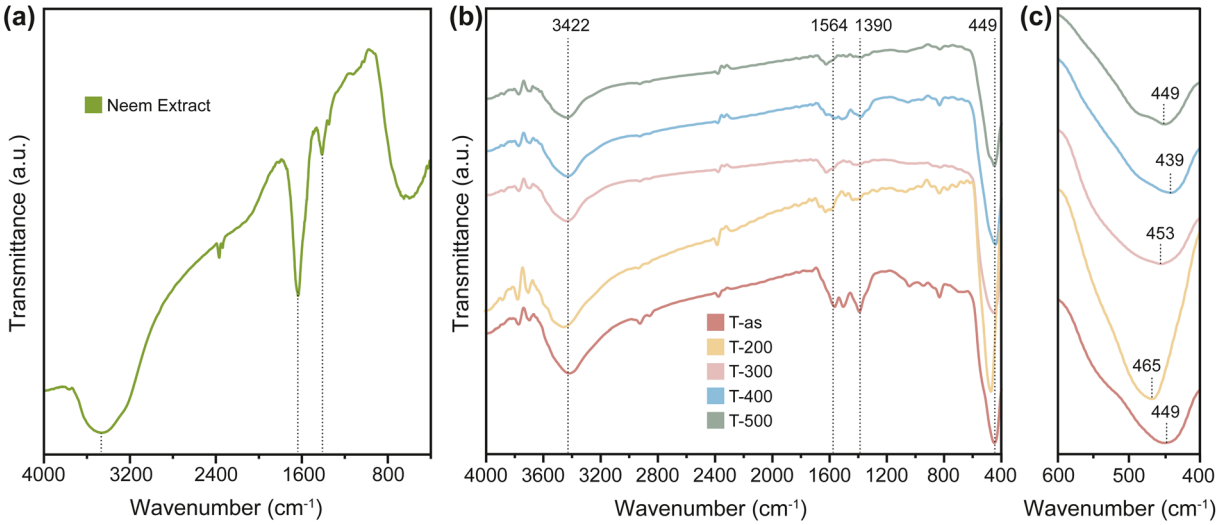

Fig. 3 FTIR spectra of (a) the leaf extract of *Azadirachta indica* representing the presence of bioactive compounds and (b) ZnO NPs annealed at different temperatures. The magnified view (c) of the spectra displays the peak shift of Zn–O due to temperature variation.

1560 cm^{-1} indicates the decomposition of the capping agents with increasing heat treatment.[23]

With increasing annealing temperature, the stretching vibrational frequency of Zn–O bonds shifts to higher values while remaining within the range of 439–465 cm^{-1}. For better visualization, a magnified view of the spectra of Zn–O bonds (600-400 cm^{-1}) is shown in Fig. 3c. The band at approximately 449 cm^{-1} in the as-synthesized sample (T-as) shifts to a higher wavenumber, around 465 cm^{-1}, for T-200. This shift to higher wavenumbers, along with a decrease in the bandwidth of the Zn–O bond compared to the sample as synthesized, indicates changes in the lattice parameters of the ZnO nanoparticles and an increase in the crystallite size.[51] However, with further increases in the annealing temperature up to 400 °C, the FTIR peak shifts to lower wavenumbers, corresponding to a reduction in particle size. Beyond this, enhanced crystallization causes the FTIR peak to shift back to higher wavenumbers, from 439 cm^{-1} to 449 cm^{-1}, upon annealing from 400 to 500 °C. This shift towards higher wavenumbers again reflects changes in the lattice parameters and particle size. These results are in corroboration with the results obtained from XRD, and FESEM, analysis, which will be discussed in the next sections. The gradual reduction in the intensity of all bands, except Zn–O in FTIR data, with an increase in the annealing temperature clearly confirms the enhanced compositional purity of the ZnO nanoparticles with rapid decomposition of bioactive compounds. The decomposition of biocompounds with increasing annealing temperature can act as a major factor for the reduction in particle size, which will be described in further detail in the FESEM results section.[16]

Structural characterizations

X-ray diffraction analysis. To examine the phase identity, crystalline nature, and purity of the synthesized NPs, XRD analysis was employed. Fig. 4a presents comparative XRD patterns of the as-synthesized ZnO sample and samples annealed at 200, 300, 400, and 500 °C. In the as-synthesized sample (without annealing), diffraction peaks are observed at 2θ values of 31.71°, 34.37°, 36.20°, 47.49°, 56.54°, 62.79°, 66.36°, 67.88°, and 68.98°, corresponding to the planes (100), (002), (101), (102), (110), (103), (200), (112), and (201), respectively. All the diffraction peaks agree well with that of the hexagonal ZnO wurtzite structure with the $P6_3mc$ space group (JCPDS, No. 36-1451). Within the detection limits of the XRD technique, no additional peaks corresponding to secondary phases or impurities are observed, confirming the formation of single-phase ZnO NPs through the eco-friendly and low-cost green synthesis route.

As the annealing temperature increases from 200 °C to 400 °C, the (101) diffraction peak broadens (Fig. 4b), indicating a reduction in crystallinity.[51] This phenomenon is likely caused by organic residues from leaf extract, which induce strain within the crystal lattice.[52,53] In contrast, as the annealing temperature increases from 400 °C to 500 °C, the prominent peaks (100), (002), and (101) show enhanced crystallinity. The full width at half maximum (FWHM) of the (101) peak decreases and the sharpness of the peaks improves, reflecting increased crystallinity and crystallite size.[51] These may be the result of the starting organic precursors having been decomposed at high annealing temperature, which has been discussed in the FTIR section.

The mean crystallite sizes (D) are calculated using the Debye–Scherrer equation,[51] given by $D = \frac{k\lambda}{\beta\cos\theta}$, where k is the Scherrer constant (typically 0.9), λ is the X-ray wavelength (1.54056 Å), θ is the Bragg angle, and β is the FWHM of the most intense diffraction peak (101). The crystallite size increases from 25.67 nm for the as-synthesized sample to 28.23 nm for the sample annealed at 200 °C, confirming improved crystallinity due to the reduction in FWHM (Fig. 4c). However, as the annealing temperature increases further, the crystallite size decreases, reaching a minimum of 22.98 nm at 400 °C, which is consistent with the observed peak broadening. At 500 °C, the

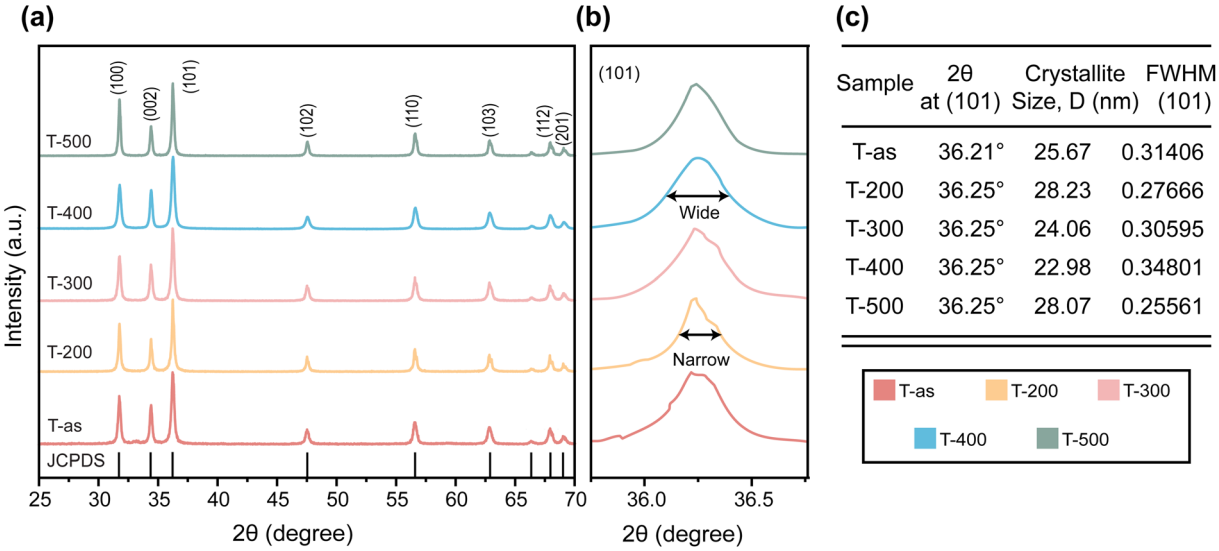

Sample	2θ at (101)	Crystallite Size, D (nm)	FWHM (101)
T-as	36.21°	25.67	0.31406
T-200	36.25°	28.23	0.27666
T-300	36.25°	24.06	0.30595
T-400	36.25°	22.98	0.34801
T-500	36.25°	28.07	0.25561

Fig. 4 (a) X-ray diffraction patterns of different ZnO NP samples, (b) XRD peaks at (101) spectra of ZnO NPs synthesized using *Azadirachta indica* leaf extract and annealed at different temperatures, highlighting structural changes, and (c) a table containing average crystallite size and FWHMs of different ZnO NP samples.

crystallite size increases again to 28.07 nm, further validating the enhanced crystallinity at this temperature. It is also observed that while the annealing temperature increases from 200 °C to 500 °C, the prominent peak slightly shifted toward lower diffraction angle (2θ) values. This slight shift in the position of the (101) peak reflects the increase in lattice parameters as thermal annealing increases.[49]

The lattice strain (ε) in different ZnO samples is estimated using Wilson's formula,[51] given by $\varepsilon = \frac{\beta}{4\tan\theta}$, where β is the FWHM and θ is the Bragg angle. The calculated strain values, summarized in Table 1, exhibit a trend consistent with the crystallite size. Specifically, at 500 °C, the strain decreases with increasing crystallite size. These findings are in good agreement with previous observations.[51]

The dislocation density (δ_{hkl}) for all samples is estimated using the relation $\delta_{hkl} = \frac{1}{D^2}$, where D is the mean crystallite size.[51] Table 1 presents the dislocation density (δ_{101}) values at the peaks (101). A notable decrease in dislocation density is observed with an increase in the annealing temperature from 400 °C to 500 °C. This reduction can be attributed to the migration of atoms from inside of the crystallites to the grain boundaries.[53] Elevated thermal energy during annealing promotes the recovery of dislocated atoms at the grain boundaries, thus reducing the overall dislocation density.[54]

The interplanar spacing (d_{101}) corresponding to the dominant (101) peak is calculated using the relation $\frac{1}{d^2} = \frac{4}{3} \times \frac{h^2 + hk + k^2}{a^2} + \frac{l^2}{c^2}$, where a and c are the lattice constants of the hexagonal crystal system.[51] Table 2 compares the estimated values d_{101} for different samples with the standard JCPDS data, together with the corresponding relative percentage errors. Among the samples, T-400 exhibits the largest difference in d_{101} (2.47868 Å) compared to the JCPDS data (2.475 Å). This deviation, coupled with the slight peak (101) shift towards higher 2θ values observed in Fig. 3c, further confirms the presence of smaller crystallite sizes in the T-400 sample.

Field emission scanning electron microscopy. To evaluate the effect of varying annealing temperature on the surface

Table 1 Structural parameters obtained from XRD analysis of as-synthesized and annealed ZnO nanoparticles at different temperatures

Sample name	Average lattice strain × 10^{-2}	Dislocation density × 10^{15} m^{-2}	Lattice parameters	
	ε	δ_{101}	$a = b$	c
T-as	0.071134219	1.41192	3.2543	5.2069
T-200	0.065046865	1.09541	3.2542	5.2068
T-300	0.074423221	1.33963	3.2544	5.207
T-400	0.079364849	1.73324	3.2545	5.2072
T-500	0.063001856	0.935039	3.2543	5.2069

Table 2 Calculated interplanar spacing for the prominent (101) peak of the XRD data for different ZnO samples and relative error corresponding to it

Sample name	Interplanar spacing for (101)		Relative error (%) in interplanar spacing
	d_{XRD} (Å)	d_{JCPDS} (Å)	
T-as	2.478532292	2.47592	0.105507951
T-200	2.478462602	2.47592	0.102693223
T-300	2.478601983	2.47592	0.108322671
T-400	2.478682459	2.47592	0.11157302
T-500	2.478532292	2.47592	0.105507951

morphologies and sizes of NPs, field emission scanning electron microscopy (FESEM) imaging was performed. Fig. 5(a–e) display the FESEM images of the size distribution of ZnO NPs. The results indicate that higher temperatures promote the development of NPs with more regular shapes. This morphological transformation is attributed to the decomposition of green precursors at elevated temperatures, which facilitates the formation of pure ZnO NPs with uniform geometries.[16] The size of as-synthesized nanoparticles is larger compared to that of T-200, which contrasts with the trend observed in the crystallite size. The size of NPs is mainly influenced by their colloidal stability rather than being solely dependent on their crystallite size.[55] Due to their lower colloidal stability, T-as nanoparticles (48.64 nm) exhibited a larger diameter compared to T-200 nanoparticles (41.95 nm). This observation will be further elaborated upon in the dynamic light scattering (DLS) analysis section. Furthermore, Fig. 5f demonstrates that the average diameter of the ZnO nanoparticles decreases from 41.95 to 27.51 nm as the annealing temperature increases from 200 to 400 °C. This trend is likely associated with the gradual removal of surface-bound phytochemicals at elevated temperatures, as also suggested by FTIR results. The reduction in organic residue may improve particle compactness and promote more defined morphologies.[16] However, beyond 400 °C, a slight increase in particle size is observed, potentially due to thermal agglomeration effects, which are common at higher annealing temperatures.[30,33]

Colloidal characterization

Dynamic light scattering (DLS) analysis. To further support the claim of FESEM results, colloidal stability was analyzed by evaluating the results of zeta potential and hydrodynamic size measurement. The zeta potential values are compiled together with the hydrodynamic size in Fig. 6. As shown in Fig. 6, the negative charge on ZnO NP gradually increases with increasing heat treatment, suggesting reduced agglomeration at elevated temperatures.[56] The as-synthesized ZnO exhibits a relatively low negative zeta potential of −8.6 mV, while NPs annealed at 400 °C and 500 °C display significantly higher negative values of −45.1 mV and −37.8 mV, respectively. The zeta potential increased with increasing annealing temperature and reached the optimal value at 400 °C. These results indicate enhanced colloidal stability for T-400 and T-500, as more negative zeta potentials promote electrostatic repulsion between particles, thus preventing aggregation.[56–58] A plausible explanation for the observed increase in negative surface charge at elevated annealing temperatures is the thermal degradation of organic capping agents or stabilizers (see FTIR results section). This process likely results in exposure of the nanoparticle surface to

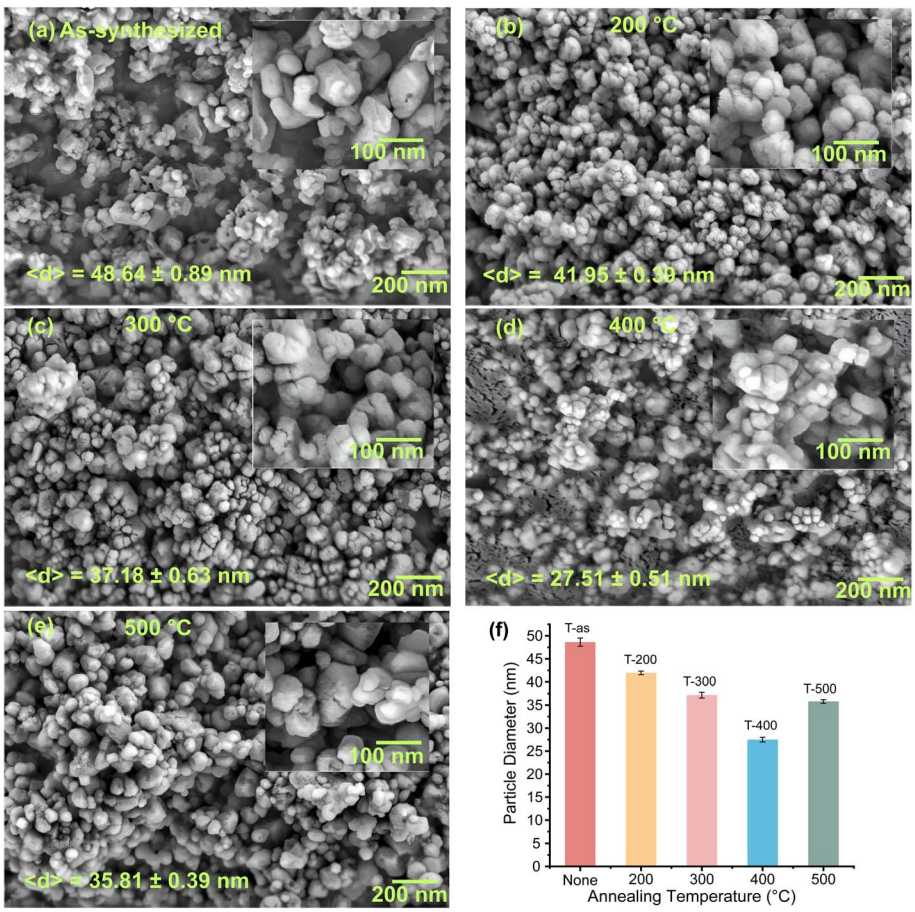

Fig. 5 SEM micrographs of (a) as-synthesized ZnO NPs, (b–e) ZnO NPs with different annealing temperatures: 200 °C, 300 °C, 400 °C, 500 °C, and (f) the comparison of particle diameters across different ZnO NP samples. The insets display the magnified view of the micrographs.

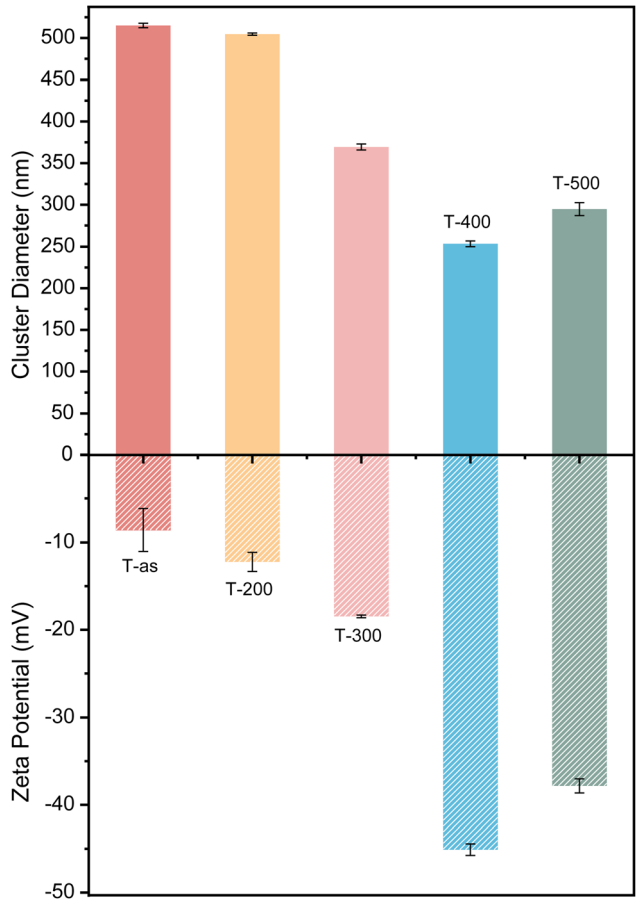

Fig. 6 Hydrodynamic size and zeta potential of ZnO NPs as-synthesized and annealed at 200 °C, 300 °C, 400 °C, and 500 °C.

negatively charged functional groups or molecular fragments, thereby enhancing the overall negative surface charge. Furthermore, T-200 NPs (−12.3 mV) exhibit greater stability compared to T-as NPs, which can be attributed to their negative zeta potential and supports the claim in the FESEM results section.

In addition to the above findings, DLS measurements provide insight into the hydrodynamic size of the ZnO NPs. At lower annealing temperatures (200 °C), the large hydrodynamic size of approximately 504 nm, almost similar to T-as (515 nm), suggests loosely aggregated nanoparticles, consistent with the lower negative value of the zeta potential. This happened because of the low electrostatic repulsion between the particles. As the annealing temperature increases to 300 °C, the diameter of the cluster decreases to around 369 nm, indicating particle disaggregation or shrinkage. The most pronounced reduction in the size of the cluster occurs at 400 °C, where the hydrodynamic size reaches a minimum of approximately 253 nm, suggesting the formation of more uniform and smaller nanoparticles. This is in agreement with the increased negative zeta potential, which promotes colloidal stability and prevents further aggregation. However, further increasing the annealing temperature to 500 °C leads to a slight increase in cluster diameter to approximately 294 nm, suggesting the onset of re-agglomeration or sintering of the nanoparticles, which is consistent with XRD and FESEM results.

Annealing-dependent performance of ZnO nanoparticles in seed priming

To investigate the annealing-dependent performance of green-synthesized ZnO nanoparticles in seed priming, bitter gourd seeds were treated with varying concentrations of ZnO NPs (60 mg L^{-1}, 120 mg L^{-1}, 250 mg L^{-1}, and 500 mg L^{-1}) for 48 hours. The results show a concentration-dependent increase in germination rate and shoot length (see Text S2 and Fig. S2, S3). Among the concentrations tested, 120 mg L^{-1} results in the most significant improvement in germination ($p < 0.001$) and shoot growth ($p < 0.001$). Therefore, this concentration is selected for further investigation into the effect of the annealing temperature on the nanopriming process.

Our results reveal a consistent and gradual improvement in seed germination and shoot length as the annealing temperature of the nanoparticles increased. Specifically, bitter gourd seeds treated with T-400 ZnO NP show a significant increase in the final germination percentage of 61.7%, 35.7%, 22.6%, and 10.1% compared to those treated with ZnO NPs T-as, T-200, T-300, and T-500, respectively (Fig. S4a and 7a). Regarding shoot length, T-400 ZnO NPs resulted in improvements of 85.3% ($p < 0.001$), 62.5% ($p < 0.001$), 47.7% ($p = 0.001$), and 51.6% ($p < 0.001$) over T-as, T-200, T-300, and T-500 ZnO NP treatments, respectively (Fig. S4b and 7b). These observations correspond well with the reduced size with an increased annealing temperature up to 400 °C. Again, the enhanced performance of the T-400 ZnO NPs can be attributed to the smaller size (27 nm).[59] These findings align with our previous research, where the smallest NPs showed the highest improvements in germination and seedling growth, concluding that variations in size and morphology contribute significantly to greater growth efficiency.[20]

Furthermore, nanopriming with T-400 ZnO nanoparticles at a concentration of 120 mg L^{-1} results in a twofold increase in both germination percentage and shoot length compared to hydropriming, demonstrating superior performance relative to previously reported studies. For example, Mazhar *et al.* report a 29% improvement in germination and a 37% increase in shoot length using 100 mg L^{-1} of commercially available ZnO nanopowder, while Kalathingal *et al.* observe respective increases of 27% and 50% with 75 mg L^{-1} of green-synthesized Ag nanoparticles.[60,61] In our earlier study, chemically synthesized ZnO nanoparticles enhance germination by 23% and shoot length by 40%.[20] The superior efficacy of T-400 is primarily attributed to enhanced zinc uptake during seed priming, enabled by its smaller particle size, which facilitates improved penetration through the seed coat and greater bioavailability of zinc.[62,63]

To verify the enhanced zinc uptake, we compare ZnO nanoparticle absorption in nanoprimed seeds with hydroprimed controls using FESEM, EDX (Fig. S5a–f), and atomic absorption spectroscopy (AAS) analysis (Text S4). FESEM imaging reveals the presence of nanoparticles embedded within the endosperm

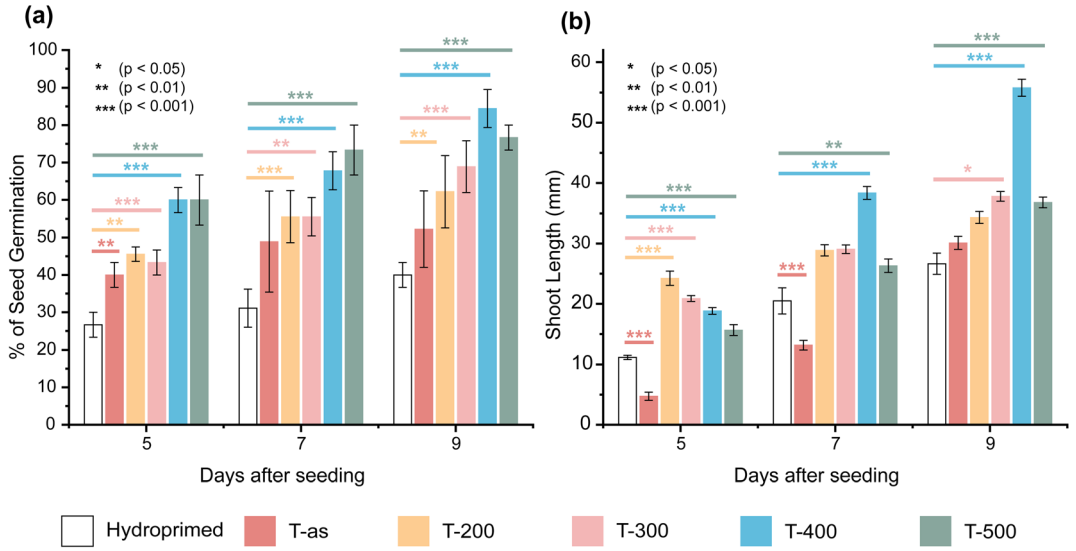

Fig. 7 Influence of green-synthesized ZnO NPs annealed at different temperatures nanopriming on (a) seed germination vigor, and (b) shoot length dynamics of bitter gourd seedlings using green synthesized ZnO NPs annealed at 200 °C, 300 °C, 400 °C, and 500 °C at 120 mg L^{-1} concentration. Data are presented as mean ± standard error of the mean based on an average of 3 sets of replication, as no significant differences were found among the triplicates containing 30 seeds each, as determined by ANOVA (see Text S3 and Table S1). Statistical differences between the mean shoot lengths of treatments (various annealing temperatures of ZnO NP priming solutions) compared to the control are denoted by (*, $p < 0.05$; **, $p < 0.01$; ***, $p < 0.001$) according to an independent sample Student's *t*-test.

of treated seeds (Fig. S5d and e), while the control seeds exhibit smooth, nanoparticle-free surfaces (Fig. S5a and b). Supporting this, EDX spectra show that nanoprimed seeds contain 0.64% zinc compared to just 0.06% in control seeds—indicating over a tenfold increase in zinc content.[64,65] Quantitative analysis using AAS further confirms this trend: the zinc concentration in nanoprimed seeds reaches levels approximately 14 times higher than those in control seeds (3.98 ppm). These results validate that ZnO NP treatment significantly enhances zinc uptake, providing a mechanistic basis for the observed improvements in seed germination and seedling development.[20,64,65]

Conclusion

This study presents, for the first time, the effect of low-temperature annealing on green-synthesized ZnO nanoparticles. A nonlinear relationship is observed between annealing temperature and particle size, with ZnO NPs annealed at 400 °C (T-400) exhibiting the smallest size, highest colloidal stability, and superior performance. Nanopriming with T-400 at 120 mg L^{-1} results in a twofold enhancement in both germination rate and shoot length compared to hydropriming. This improvement is strongly linked to increased zinc uptake and better nanoparticle penetration through the seed coat, as confirmed by FESEM, EDX, and AAS analyses. Although the optimal concentration for bitter gourd is consistent, it might differ for other plant species, indicating a need for additional research. Our results highlight the crucial role of thermal tuning in nanoparticle engineering and demonstrate the promise of green nanotechnology as a sustainable and effective strategy for enhancing crop productivity.

Conflicts of interest

The authors declare no conflicts of interest.

Data availability

All data supporting the findings of this study are available within the main manuscript and the SI.

Text S1: Optical studies of ZnO NPs by UV-vis spectrophotometer. Text S2: Effect of nanopriming with ZnO nanoparticles on germination and seedling parameters of bitter gourd seed at different concentrations. Text S3: A one way ANOVA analysis for bitter gourd. Text S4: Internalization studies of Zn content in primed seeds. Fig. S1: Characterization studies of ZnO NPs synthesized from *Azadirachta indica* leaf aqueous extract, (a) UV-visible absorption spectra of the ZnO NPs and (b) energy dispersive X-ray (EDX) elemental analysis of ZnO NPs. (c) A blank experiment conducted without neem extract resulted in no peak for ZnO in UV-vis spectra. Fig. S2: Effect of ZnO NPs priming on the dynamic of seed germination rate of bitter gourd. Germination rate for (a) 500 °C, (b) 400 °C, (c) 300 °C, and (d) 200 °C annealed ZnO NPs at the concentrations of 60 mg L^{-1}, 120 mg L^{-1}, 250 mg L^{-1}, and 500 mg L^{-1}. Data are presented as means of three replicates containing 30 seeds each ± standard error of means. Statistical differences between the mean of treatments (various concentrations of ZnO NP priming solutions) compared to the control are denoted by (*, $p < 0.05$; **, $p < 0.01$; ***, $p < 0.001$) according to an Independent sample Student's *t*-test. Fig. S3: Effect of ZnO NPs priming on the dynamic of shoot length of bitter gourd seeds. Shoot length for (a) 500 °C, (b) 400 °C, (c) 300 °C, and (d) 200 °C annealed ZnO NPs at the concentrations of 60 mg L^{-1}, 120 mg L^{-1}, 250 mg L^{-1},

and 500 mg L^{-1}. Data are presented as means of three replicates containing 30 seeds each ± standard error of means. Statistical differences between the mean of treatments (various concentrations of ZnO NP priming solutions) compared to the control are denoted by (*, $p < 0.05$; **, $p < 0.01$; ***, $p < 0.001$) according to an Independent sample Student's *t*-test. Fig. S4: Comparison of nanopriming results between as-synthesized and annealed at 400 °C ZnO NPs in (a) germination percentage and (b) shoot length. Fig. S5: FESEM images of bitter gourd seed surfaces and embryos. (a and b) Control (hydroprimed) seeds, (c) EDX spectrum of control seed, (d and e) ZnO NP-treated seeds, and (f) EDX spectrum of ZnO NP-treated seed. Table S1: *p*-values obtained from one way ANOVA between triplicates for bitter gourd nanoprimed at 120 mg L^{-1} concentration with ZnO NPs annealed at different temperatures. See DOI: **https://doi.org/10.1039/d5na00354g**.

Acknowledgements

Ahsan Habib acknowledges the Ministry of Science and Technology Research Grant 2024-2025 (SRG-242301). Mahmudur Rahman acknowledges the University Grants Commission of Bangladesh Research Grant 2024-2025 University Grant Commission, DUET, Gazipur (CASR No. 79). The authors extend sincere thanks for the synthesis facilities provided by the Semiconductor Technology Research Center (STRC). The appreciation is also due to the Department of Biomedical Engineering at the Bangladesh University of Engineering and Technology for facilitating the FESEM studies. The authors appreciate the valuable support from the Centre for Advanced Research in Sciences (CARS) for XRD and FTIR analysis. The authors also thank Dr Sharnali Islam for her valuable input and insightful discussions that contributed to the conceptual development of this study. Finally, the authors acknowledge Professor Md. Nurul Amin for AAS analysis and Bangladesh Council of Scientific and Industrial Research (BCSIR) for XPS analysis.

References

1 FOOD, O., *The State of Food and Agriculture*, Climate change, agri, 2016.
2 M. Kah, N. Tufenkji and J. C. White, Nano-enabled strategies to enhance crop nutrition and protection, *Nat. Nanotechnol.*, 2019, **14**, 532–540.
3 V. W. Ruttan, Productivity growth in world agriculture: sources and constraints, *J. Econ. Perspect.*, 2002, **16**, 161–184.
4 L. Zhao, L. Lu, A. Wang, H. Zhang, M. Huang, H. Wu, B. Xing, Z. Wang and R. Ji, Nano-biotechnology in agriculture: use of nanomaterials to promote plant growth and stress tolerance, *J. Agric. Food Chem.*, 2020, **68**, 1935–1947.
5 X. Ma and P. Zhou, Promising prospects of nanomaterials in crop safety, *Nat. Food*, 2024, **5**, 886–887.
6 S. K. Verma, A. K. Das, M. K. Patel, A. Shah, V. Kumar and S. Gantait, Engineered nanomaterials for plant growth and development: a perspective analysis, *Sci. Total Environ.*, 2018, **630**, 1413–1435.
7 I. Ocsoy, M. L. Paret, M. A. Ocsoy, S. Kunwar, T. Chen, M. You and W. Tan, Nanotechnology in plant disease management: DNA-directed silver nanoparticles on graphene oxide as an antibacterial against Xanthomonas perforans, *ACS Nano*, 2013, **7**, 8972–8980.
8 M. H. Siddiqui, M. H. Al-Whaibi, M. Firoz and M. Y. Al-Khaishany, Role of nanoparticles in plants, *Nanotechnology and plant sciences: nanoparticles and their impact on plants*, 2015, pp. 19–35.
9 L. Sun, Y. Wang, R. Wang, R. Wang, P. Zhang, Q. Ju and J. Xu, Physiological, transcriptomic, and metabolomic analyses reveal zinc oxide nanoparticles modulate plant growth in tomato, *Environ. Sci.: Nano*, 2020, **7**, 3587–3604.
10 J. Hu, C. Gong, Y. Jia, H. Feng, J. Chen, G. Qin, A. Liang, A. Peng, Y. Huang and M. Sun, others Preparation of pH-Responsive Kas@ ZnO Quantum Dots for Synergistic Control of Rice Blast and Enhanced Disease Resistance in Rice, *ACS Appl. Mater. Interfaces*, 2024, **16**, 60842–60855.
11 J. Lian, L. Cheng, X. Wang, Y. Chen, C. Deng, Y. Wang, J. Pan, M. J. I. Shohag, X. Xin and Z. He, others Bespoke ZnO NPs Synthesis Platform to Optimize Their Performance for Improving the Grain Yield, Zinc Biofortification, and Cd Mitigation in Wheat, *ACS Sustain. Chem. Eng.*, 2024, **12**, 716–727.
12 E. A. Meulenkamp, Synthesis and growth of ZnO nanoparticles, *J. Phys. Chem. B*, 1998, **102**, 5566–5572.
13 S. Faisal, H. Jan, S. A. Shah, S. Shah, A. Khan, M. T. Akbar, M. Rizwan, F. Jan, Wajidullah, N. Akhtar, *et al.*, Green synthesis of zinc oxide (ZnO) nanoparticles using aqueous fruit extracts of Myristica fragrans: their characterizations and biological and environmental applications, *ACS Omega*, 2021, **6**, 9709–9722.
14 A. Naveed Ul Haq, A. Nadhman, I. Ullah, G. Mustafa, M. Yasinzai and I. Khan, Synthesis approaches of zinc oxide nanoparticles: the dilemma of ecotoxicity, *J. Nanomater.*, 2017, **2017**, 8510342.
15 J. Iqbal, B. A. Abbasi, T. Yaseen, S. A. Zahra, A. Shahbaz, S. A. Shah, S. Uddin, X. Ma, B. Raouf and S. Kanwal, others Green synthesis of zinc oxide nanoparticles using Elaeagnus angustifolia L. leaf extracts and their multiple in vitro biological applications, *Sci. Rep.*, 2021, **11**, 20988.
16 N. Bala, S. Saha, M. Chakraborty, M. Maiti, S. Das, R. Basu and P. Nandy, Green synthesis of zinc oxide nanoparticles using Hibiscus subdariffa leaf extract: effect of temperature on synthesis, anti-bacterial activity and anti-diabetic activity, *RSC Adv.*, 2015, **5**, 4993–5003.
17 N. Senthilkumar, E. Nandhakumar, P. Priya, D. Soni, M. Vimalan and I. V. Potheher, Synthesis of ZnO nanoparticles using leaf extract of Tectona grandis (L.) and their anti-bacterial, anti-arthritic, anti-oxidant and in vitro cytotoxicity activities, *New J. Chem.*, 2017, **41**, 10347–10356.
18 P. Porrawatkul, R. Pimsen, A. Kuyyogsuy, N. Teppaya, A. Noypha, S. Chanthai and P. Nuengmatcha, Microwave-assisted synthesis of Ag/ZnO nanoparticles using Averrhoa carambola fruit extract as the reducing agent and their application in cotton fabrics with antibacterial and UV-protection properties, *RSC Adv.*, 2022, **12**, 15008–15019.

19 R. Septiyani and C. Wibowo, Identification of active compounds and testing the antioxidant properties of neem leaf extract, *AIP Conf. Proc.*, 2019, **2094**, 020034.
20 S. Yeasmin, A. R. Dipto, A. B. Zakir, S. D. Shovan, M. A. H. Suvo, M. A. Bhuiyan, M. N. Amin, T. U. Rashid, S. Islam and A. Habib, Nanopriming and AI for Sustainable Agriculture: Boosting Seed Germination and Seedling Growth with Engineered Nanomaterials, and Smart Monitoring through Deep Learning, *ACS Appl. Nano Mater.*, 2024, **7**, 8703–8715.
21 J. Borgatta, C. Ma, N. Hudson-Smith, W. Elmer, C. D. Plaza Pérez, R. De La Torre-Roche, N. Zuverza-Mena, C. L. Haynes, J. C. White and R. J. Hamers, Copper Based Nanomaterials Suppress Root Fungal Disease in Watermelon (Citrullus lanatus): Role of Particle Morphology, Composition and Dissolution Behavior, *ACS Sustainable Chem. Eng.*, 2018, **6**, 14847–14856.
22 J. Borgatta, Y. Shen, C. Tamez, C. Green, J. K. Hedlund Orbeck, M. S. Cahill, C. Protter, C. Deng, Y. Wang, W. Elmer, J. C. White and R. J. Hamers, Influence of CuO Nanoparticle Aspect Ratio and Surface Charge on Disease Suppression in Tomato (Solanum lycopersicum), *J. Agric. Food Chem.*, 2023, **71**, 9644–9655.
23 B. Naiel, M. Fawzy, M. W. A. Halmy and A. E. D. Mahmoud, Green synthesis of zinc oxide nanoparticles using Sea Lavender (Limonium pruinosum L. Chaz.) extract: characterization, evaluation of anti-skin cancer, antimicrobial and antioxidant potentials, *Sci. Rep.*, 2022, **12**, 20370.
24 M. H. Kahsay, A. Tadesse, D. RamaDevi, N. Belachew and K. Basavaiah, Green synthesis of zinc oxide nanostructures and investigation of their photocatalytic and bactericidal applications, *RSC Adv.*, 2019, **9**, 36967–36981.
25 M. Aliannezhadi, F. Doost Mohamadi, M. Jamali and F. Shariatmadar Tehrani, Ultrasound-assisted green synthesized zno nanoparticles with different solution ph for water treatment, *Sci. Rep.*, 2025, **15**, 7203.
26 R. Hamed, R. Z. Obeid and R. Abu-Huwaij, Plant mediated-green synthesis of zinc oxide nanoparticles: An insight into biomedical applications, *Nanotechnol. Rev.*, 2023, **12**, 20230112.
27 T. S. Aldeen, H. E. Ahmed Mohamed and M. Maaza, ZnO nanoparticles prepared via a green synthesis approach: Physical properties, photocatalytic and antibacterial activity, *J. Phys. Chem. Solids*, 2022, **160**, 110313.
28 V. Beermann, M. Gocyla, S. Kühl, E. Padgett, H. Schmies, M. Goerlin, N. Erini, M. Shviro, M. Heggen and R. E. Dunin-Borkowski, others Tuning the electrocatalytic oxygen reduction reaction activity and stability of shape-controlled Pt–Ni nanoparticles by thermal annealing-elucidating the surface atomic structural and compositional changes, *J. Am. Chem. Soc.*, 2017, **139**, 16536–16547.
29 K. Park, Q. Zhang, B. B. Garcia and G. Cao, Effect of annealing temperature on TiO2- ZnO core- shell aggregate photoelectrodes of dye-sensitized solar cells, *J. Phys. Chem. C*, 2011, **115**, 4927–4934.
30 V. Noack and A. Eychmüller, Annealing of nanometer-sized zinc oxide particles, *Chem. Mater.*, 2002, **14**, 1411–1417.
31 M. Miyauchi, A. Ikezawa, H. Tobimatsu, H. Irie and K. Hashimoto, Zeta potential and photocatalytic activity of nitrogen doped TiO 2 thin films, *Phys. Chem. Chem. Phys.*, 2004, **6**, 865–870.
32 T. Bhuyan, K. Mishra, M. Khanuja, R. Prasad and A. Varma, Biosynthesis of zinc oxide nanoparticles from Azadirachta indica for antibacterial and photocatalytic applications, *Mater. Sci. Semicond. Process.*, 2015, **32**, 55–61.
33 K. Elumalai and S. Velmurugan, Green synthesis, characterization and antimicrobial activities of zinc oxide nanoparticles from the leaf extract of Azadirachta indica (L.), *Appl. Surf. Sci.*, 2015, **345**, 329–336.
34 I. L. Ikhioya and A. C. Nkele, Green synthesis and characterization of aluminum oxide nanoparticle using neem leaf extract (Azadirachta Indica), *Hybrid Adv.*, 2024, **5**, 100141.
35 A. Singh and M. Kaushik, others Physicochemical investigations of zinc oxide nanoparticles synthesized from Azadirachta Indica (Neem) leaf extract and their interaction with Calf-Thymus DNA, *Results Phys.*, 2019, **13**, 102168.
36 B. Adhikari, P. R. Dhital, S. Ranabhat and H. Poudel, Effect of seed hydro-priming durations on germination and seedling growth of bitter gourd (Momordica charantia), *PLoS One*, 2021, **16**, e0255258.
37 A. Powell, What is seed quality and how to measure it. Responding to the challenges of a changing world: The role of new plant varieties and high quality seed in agriculture, *Proceedings of the Second World Seed Conference*, Rome, 2009, pp. 8–10.
38 M. N. Khan, C. Fu, J. Li, Y. Tao, Y. Li, J. Hu, L. Chen, Z. Khan, H. Wu and Z. Li, Seed nanopriming: How do nanomaterials improve seed tolerance to salinity and drought?, *Chemosphere*, 2023, **310**, 136911.
39 D. Mishra, M. K. Chitara, S. Negi, J. Pal singh, R. Kumar and P. Chaturvedi, Biosynthesis of zinc oxide nanoparticles via leaf extracts of Catharanthus roseus (L.) G. Don and their application in improving seed germination potential and seedling vigor of Eleusine coracana (L.) Gaertn, *Adv. Agric.*, 2023, **2023**, 7412714.
40 Y. A. Selim, M. A. Azb, I. Ragab and M. H. M. Abd El-Azim, Green synthesis of zinc oxide nanoparticles using aqueous extract of Deverra tortuosa and their cytotoxic activities, *Sci. Rep.*, 2020, **10**, 3445.
41 L. Guo, S. Yang, C. Yang, P. Yu, J. Wang, W. Ge and G. K. Wong, Synthesis and characterization of poly(vinylpyrrolidone)-modified zinc oxide nanoparticles, *Chem. Mater.*, 2000, **12**, 2268–2274.
42 D. K. Bhui, H. Bar, P. Sarkar, G. P. Sahoo, S. P. De and A. Misra, Synthesis and UV–vis spectroscopic study of silver nanoparticles in aqueous SDS solution, *J. Mol. Liq.*, 2009, **145**, 33–37.
43 M. Sharma, S. Yadav, N. Ganesh, M. M. Srivastava and S. Srivastava, Biofabrication and characterization of flavonoid-loaded Ag, Au, Au–Ag bimetallic nanoparticles

using seed extract of the plant Madhuca longifolia for the enhancement in wound healing bio-efficacy, *Prog. Biomater.*, 2019, **8**, 51–63.

44 M. Zare, K. Namratha, S. Alghamdi, Y. H. E. Mohammad, A. Hezam, M. Zare, Q. A. Drmosh, K. Byrappa, B. N. Chandrashekar and S. Ramakrishna, others Novel green biomimetic approach for synthesis of ZnO-Ag nanocomposite; antimicrobial activity against food-borne pathogen, biocompatibility and solar photocatalysis, *Sci. Rep.*, 2019, **9**, 8303.

45 X. Yang, A. Wolcott, G. Wang, A. Sobo, R. C. Fitzmorris, F. Qian, J. Z. Zhang and Y. Li, Nitrogen-doped ZnO nanowire arrays for photoelectrochemical water splitting, *Nano Lett.*, 2009, **9**, 2331–2336.

46 A. F. Borzyszkowska, A. Sulowska, P. Czaja, A. Bielicka-Giełdoń, I. Zekker and A. Zielińska-Jurek, ZnO-decorated green-synthesized multi-doped carbon dots from Chlorella pyrenoidosa for sustainable photocatalytic carbamazepine degradation, *RSC Adv.*, 2023, **13**, 25529–25551.

47 T. K. O. Le, M. G. Mapari and T. Kim, Hedgehog Zinc Oxide–Graphene Quantum Dot Heterostructures as Photocatalysts for Visible-Light-Driven Water Splitting, *ACS Omega*, 2024, **9**, 40790–40800.

48 D. M. Nzilu, E. S. Madivoli, D. S. Makhanu, S. I. Wanakai, G. K. Kiprono and P. G. Kareru, Green synthesis of copper oxide nanoparticles and its efficiency in degradation of rifampicin antibiotic, *Sci. Rep.*, 2023, **13**, 14030.

49 R. N. Aljawfi, M. J. Alam, F. Rahman, S. Ahmad, A. Shahee and S. Kumar, Impact of annealing on the structural and optical properties of ZnO nanoparticles and tracing the formation of clusters via DFT calculation, *Arabian J. Chem.*, 2020, **13**, 2207–2218.

50 S. Kummara, M. B. Patil and T. Uriah, Synthesis, characterization, biocompatible and anticancer activity of green and chemically synthesized silver nanoparticles–a comparative study, *Biomed. Pharmacother.*, 2016, **84**, 10–21.

51 P. Kumari, A. Srivastava, R. K. Sharma, A. Saini, D. Sharma, J. S. Tawale and S. K. Srivastava, Facile synthesis and tailoring the structural and photoluminescence properties of ZnO nanoparticles via annealing in air atmosphere, *Mater. Today Commun.*, 2022, **32**, 103845.

52 S. Azizi, R. Mohamad, A. Bahadoran, S. Bayat, R. A. Rahim, A. Ariff and W. Z. Saad, Effect of annealing temperature on antimicrobial and structural properties of bio-synthesized zinc oxide nanoparticles using flower extract of Anchusa italica, *J. Photochem. Photobiol., B*, 2016, **161**, 441–449.

53 R. P. Singh, I. Hudiara and S. B. Rana, Effect of calcination temperature on the structural, optical and magnetic properties of pure and Fe-doped ZnO nanoparticles, *Mater. Sci.-Pol.*, 2016, **34**, 451–459.

54 S. Jafari and Z. Ebrahimpour, Enhanced photoresponse of annealed ZnO nanoparticle film near its bandgap, *Appl. Phys. A: Mater. Sci. Process.*, 2023, **129**, 862.

55 G. Wiese and T. W. Healy, Effect of particle size on colloid stability, *Trans. Faraday Soc.*, 1970, **66**, 490–499.

56 A. Mahajan and E. Ramana, Patents on Magnetoelectric Multiferroics and their Processing by Electrophoretic Deposition, *Recent Pat. Mater. Sci.*, 2014, **7**, 109–130.

57 A. H. Shah and M. A. Rather, Effect of calcination temperature on the crystallite size, particle size and zeta potential of TiO2 nanoparticles synthesized via polyol-mediated method, *Mater. Today: Proc.*, 2021, **44**, 482–488.

58 V. Uskoković, Dynamic light scattering based microelectrophoresis: main prospects and limitations, *J. Dispersion Sci. Technol.*, 2012, **33**, 1762–1786.

59 E. Yusefi-Tanha, S. Fallah, A. Rostamnejadi and L. R. Pokhrel, Zinc oxide nanoparticles (ZnONPs) as a novel nanofertilizer: Influence on seed yield and antioxidant defense system in soil grown soybean (Glycine max cv. Kowsar), *Sci. Total Environ.*, 2020, **738**, 140240.

60 M. W. Mazhar, M. Ishtiaq, M. Maqbool, E. A. Mahmoud, F. Ullah and H. O. Elansary, Optimizing bitter gourd (Momordica charantia L.) performance: exploring the impact of varied seed priming durations and zinc oxide nanoparticle concentrations on germination, growth, phytochemical attributes, and agronomic outcomes, *Cogent Food Agric.*, 2024, **10**, 2313052.

61 S. B. Kalathingal and D. Palengara, Influence of nanopriming with phytosynthesized silver nanoparticles on seed germination and seedling growth performance in Cucurbitaceae species, *Discover Plants*, 2025, **2**, 190.

62 M. N. Ashwini, H. P. Gajera, D. G. Hirpara, D. D. Savaliya and U. K. Kandoliya, Comparative impact of seed priming with zinc oxide nanoparticles and zinc sulphate on biocompatibility, zinc uptake, germination, seedling vitality, and antioxidant modulation in Groundnut, *J. Nanopart. Res.*, 2024, **26**, 235.

63 H. Agarwal, S. Menon, S. Venkat Kumar and S. Rajeshkumar, Mechanistic study on antibacterial action of zinc oxide nanoparticles synthesized using green route, *Chem.-Biol. Interact.*, 2018, **286**, 60–70.

64 P. D. Itroutwar, G. Kasivelu, V. Raguraman, K. Malaichamy and S. K. Sevathapandian, Effects of biogenic zinc oxide nanoparticles on seed germination and seedling vigor of maize (Zea mays), *Biocatal. Agric. Biotechnol.*, 2020, **29**, 101778.

65 P. D. Itroutwar, K. Govindaraju, S. Tamilselvan, M. Kannan, K. Raja and K. S. Subramanian, Seaweed-based biogenic ZnO nanoparticles for improving agro-morphological characteristics of rice (Oryza sativa L.), *J. Plant Growth Regul.*, 2020, **39**, 717–728.